AIChE

Inception and Termination of the Core-Annular Flow Pattern for Oil-Water Downflow Through a Vertical Pipe

Sumana Ghosh and Gargi Das
Dept. of Chemical Engineering, IIT Kharagpur 721302, India

Prasanta Kumar Das
Dept. of Mechanical Engineering, IIT Kharagpur 721302, India

DOI 10.1002/aic.12741
Published online October 21, 2011 in Wiley Online Library (wileyonlinelibrary.com).

Different flow patterns for lube oil–water and for kerosene-water downflow through a vertical glass tube have been analyzed with the help of flow visualization. Core-annular flow is the dominant flow regime, with oil forming the core, and water is forming the wall film. When the velocities are increased, transition to slug flow and transition to dispersed flow are found. The waves found during the transition to slug flow depend on oil viscosity: axisymmetric bamboo waves are seen in kerosene-water downflow and the waves are asymmetric in case of lube oil–water flow where they have a cork-screw shape. Based on the experimental observations, simple mathematical models have been proposed for predicting the flow pattern transition curves. © 2011 American Institute of Chemical Engineers *AIChE J,* 58: 2020–2029, 2012
Keywords: multiphase-flow, oil–water downflow, transition criteria, flow regimes, core-, annular flow

Introduction

Liquid-liquid two-phase flow is found in many industrial applications, like chemical processes, multiphase reactors and during the production and transport of oil. In all these applications, the distribution of the two liquids inside the pipeline within a specific flow regime and transition between various flow regimes determine the transport properties, such as the pressure drop and the holdup of the phases. Therefore, knowledge of the flow patterns and an understanding of the transition mechanisms between the flow regimes are necessary for a proper design and operation of liquid-liquid flow in pipelines. In the past few decades a number of studies for oil–water transport in pipelines were published. The studies on experimental estimation of flow patterns and theoretical prediction of transition criteria reveals that the researchers have used oils with different properties and have observed the flow patterns to vary with the oil–water throughput, the physical properties (density, viscosity and interfacial tension), the pipe diameter, the pipe wall material (hydrophilic or hydrophobic) and the pipe orientation. For example, stratified flow can be observed in case of horizontal flow of low-viscosity oil and water, while it is hardly observed for high-viscosity oil–water systems. The core-annular flow pattern is a common occurrence for high-viscosity oil, but only a few researchers have reported this pattern for low-viscosity oil–water flows. Similarly the dispersed flow pattern comprising of oil dispersed and water dispersed distributions are more common for low-viscous oil–water flow due to their low-interfacial tension. Nevertheless, almost every past study has considered a specific oil–water pair, instead of explicitly analyzing the effect of a range of oil properties on the oil–water transport. In addition, theoretical studies on modeling the transition criteria are primarily confined to the onset and termination of the stratified flow regime.

One of the earliest theoretical studies on liquid-liquid flow pattern transition was reported by Brauner and Moalem Maron[1] for horizontal flow. They have predicted the transition from the stratified and annular flow regimes based on linear stability analysis performed on transient two-fluid model. The annular flow to slug flow transition is proposed to occur at a critical holdup of 0.5. They have considered experimental data of Russell et al.[2] (μ = 0.018 Pa-s, and ρ = 834 kg/m^3, pipe dia. D = 0.0205 m) and Guevara et al.[3] (μ = 10 Pa-s, and ρ = 995 kg/m^3, pipe dia. D = 0.203 m) for validating their model. Recently Grassi et al.[4] have noticed that the proposition by Brauner and Maron[1] to apply a critical holdup fraction of 0.5 gave a poor estimate for the prediction of the transition from core annular flow to slug flow. Trallero[5] observed that the transition criteria developed for gas-liquid systems were inadequate for horizontal oil–water system. Accordingly, he proposed new transition criteria for the stratified and three-layer flow pattern based on Kelvin-Helmoholtz instability mechanism for oil (μ = 0.0296 Pa-s, and ρ = 850 kg/m^3)—water horizontal flow through an acrylic resin pipe of dia. 0.05 m. He reported that due to Kelvin-Helmoholtz instability interfacial waves increased in amplitude during stratified flow and the wavelength decrease with increase in phase velocities. Brauner[6] has modified the theory of Hinze[7] to predict the transition to gas-liquid and liquid-liquid dispersed flows. The model proposes dispersion to exist if the stable bubble diameter is less than the critical diameter. She has noted that phase

Correspondence concerning this article should be addressed to G. Das at gargi@che.iitkgp.ernet.in.

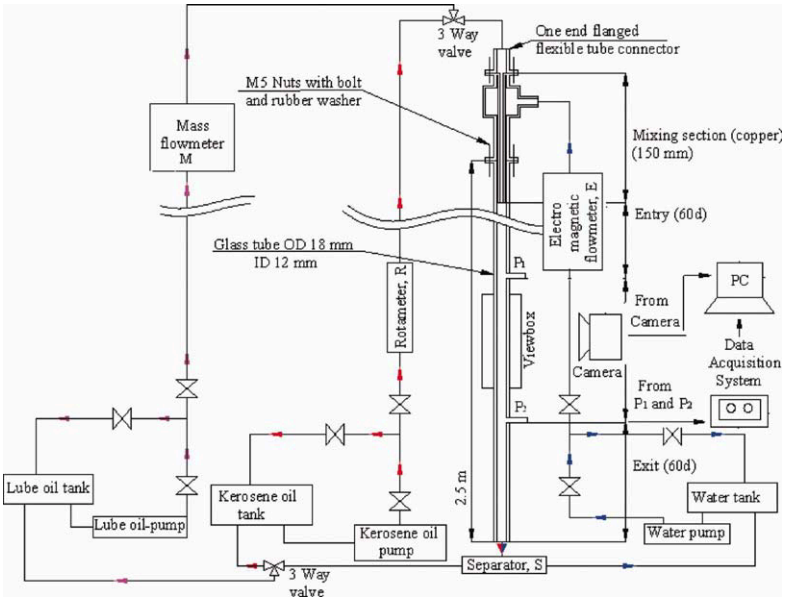

Figure 1. Schematic of experimental setup.

[Color figure can be viewed in the online issue, which is available at wileyonlinelibrary.com.]

velocities, density and viscosity ratio expressed as suitable nondimensional numbers (Reynolds, Weber and Eötvös) influence the bubble diameter in liquid-liquid flow, and, thereby affects the transition criterion of dispersed flow. The models agreed well with reported literature data for different pipe inclination, orientation and fluid properties. Later Brauner[8] reviewed the transition criteria proposed for different liquid-liquid flow regimes. Al-Wahaibi and Angeli[9] have proposed a model based on Kelvin-Helmoholtz instability mechanism to predict the critical amplitude of interfacial waves responsible for transition from stratified to nonstratified regimes in case of horizontal oil–water flow. They have noted that the criterion of critical amplitude is different for low- and high-viscosity oils. For low-viscosity oils it occurs when the slip between the phases is negligible, while for high-viscosity oils it appears when the water velocity exceeds the oil velocity. Recently Sotgia et al.[10] obtained flow regime maps for horizontal flow of high-viscosity oil and water in different diameter pyrex and plexiglas pipes. They observed that the locus of maximum reduction factor is close to annular stratified transition boundary for high-viscous oil–water horizontal flow. From their experimental observations, they proposed an empirical correlation to predict the transition between stratified flow and annular flow based on minimum mixture momentum transported during core-annular flow. They concluded that the transition depend on the fluid properties, but is independent of pipe diameter.

Thus, it can be said that the prediction of flow pattern transitions in oil–water pipelines is a complex hydrodynamic problem. The transition criteria for gas-liquid flow cannot directly be applied to such systems in a straightforward manner, and also a unified approach for oils of different properties is difficult. In addition, the majority of the investigations has been conducted either on horizontal or vertical upflow of the two liquids. Very little information is available for vertical downflow of oil–water mixtures. The only studies have been reported by Bai et al.[11] and Liu et al.[12] to the best of the authors' knowledge. The former have reported the flow patterns during up and downflow of oil (μ = 0.6 Pa-s, and ρ = 905 kg/m^3), and water through a 0.009525 m dia. glass pipe shaped as an inverted U tube, and the latter have noted the flow patterns and their transitions for 39 wt % aqueous calcium chloride solution and Exxol oil D80 using laser-induced fluorescence.

In this article, the flow patterns for oil–water downflow through a vertical pipe are measured. Both high-viscosity and low-viscosity oils have been considered to determine the influence of the physical properties of oil on the flow characteristics. Our experimental observations have revealed that core-annular flow is the dominating flow pattern for both oil viscosities, but there are distinct differences in the core flow characteristics for low-viscosity and high-viscosity oil. This gives rise to different flow pattern transitions when the phase velocities are changed. Based on our experimental observations, different physical mechanisms have been suggested for the inception and termination of the core-annular flow pattern. Using simplified mathematical analysis, transition criteria for the different flow regimes have been developed and the model predictions are compared with the experimental observations.

Experimental setup and procedure

A schematic of the experimental setup is presented in Figure 1. The test rig for vertical downflow comprises of a glass pipe of 0.012 m dia. with 2.5 m length. The test fluids used in the experiments are lubricating oil (μ = 0.2 Pa-s, ρ = 960 kg/m^3, σ = 0.039 N/m), kerosene (= 0.0012 Pa-s, = 787 kg/m^3, = 0.027 N/m), and water (μ = 0.001 Pa-s, ρ = 1000 kg/m^3, σ = 0.072 N/m). Kerosene is dyed for a better visualization of the flow phenomena through the transparent test section. Lube oil is pumped by a high-head gear pump, while centrifugal pumps are used for water and kerosene. The flow rate of the test fluids are measured with an electromagnetic flow meter (E) for water, a Coriolis mass flow meter (M) for lube oil, and rotameters (R) for kerosene. The specifications of the individual meters and the measurement accuracy are also mentioned in Table 1 along with the

Table 1. Range and Accuracy of Flow Meters

Fluid used	Flow meter	Range (m^3/s)	Accuracy	Experimental range of phase velocities (m/s)
Lube oil	Coriolis	0 to $3.33X10^{-4}$	±0.8%	0.075-0.8
Kerosene	Rotameter	0 to $1.67X10^{-4}$	± 2%	0.075-1.2
Water	Electromagnetic	0 to $4.17X10^{-4}$	± 0.5%	0.15-1.6

experimental velocity range adopted for each liquid used in this study.

A three-way valve directs the flow of either lube oil or kerosene into the central portion of a specially designed copper nozzle and water is injected into the annular passage between the nozzle and pipe wall. The nozzle design, thus, ensures core flow at the entry. Fluids enter the separator (S) after flowing through the test and exit sections—here they are gravity separated and recycled back to their respective storage tanks.

The flow regimes are observed visually and photographed at a distance of 1 m (L/D = 83) from the inlet. A digital camera (DSCH9, SONY) is used for photographic recording of the flow phenomena at different superficial velocities of both the phases. A view box filled with water is placed at this position to correct for the optical distortions induced by the pipe wall curvature and to allow for easy observation and camera recording.

The pressure drop is measured between two taps 0.7 m apart by a differential pressure transmitter (Honeywell -STD 120 Type). It has a pressure range of 70 kPa and full-scale accuracy of ±0.5%. The tubes connecting the taps to the transmitter are filled with water and during experiments it is ensured that no oil enters the pressure line. The differential data $-\left(\frac{dp}{dz}\right)_{diff}$ is used to estimate the frictional pressure gradient as follows since this can be related to the energy loss during such transportation

$$\left(-\frac{dp}{dz}\right)_f = \left(\frac{dp}{dz}\right)_{diff} - H_o(\rho_w - \rho_o)g \tag{1}$$

In Eq. 1 g, ρ_w, ρ_o, are the acceleration due to gravity, densities of water and oil, respectively. H_o is the *in situ* volume fraction of oil.

H_o for both the systems is calculated using the empirical correlation proposed by Arney et al.[13] viz

$$\begin{aligned} H_w &= \beta_w[1 + 0.35(1 - \beta_w)] \\ H_o &= 1 - H_w \end{aligned} \tag{2}$$

β_w is the inlet volume fraction of water defined as

$$\beta_w = \frac{Q_w}{Q_o + Q_w} \tag{3}$$

where Q_w and Q_o are the measured volumetric flow rates of water and oil, respectively.

The frictional pressure drop as estimated from Eq. 1 lies within 1–14% of the overall, drop and the minimum overall drop has been recorded as 15.3 Pa. Therefore, to ensure that the error in measurement is less than the frictional pressure drop even for the lowest overall pressure drop reading, pressure transducers with a least count of 0.5 Pa has been used for the experiments.

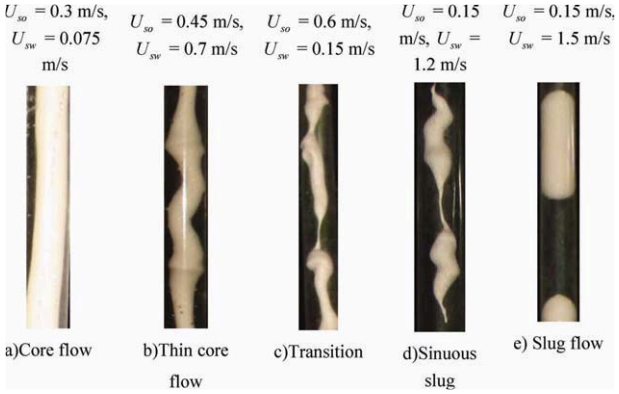

Figure 2. Representative photographs of lube oil–water flow.

[Color figure can be viewed in the online issue, which is available at wileyonlinelibrary.com.]

The error in calculation of H_w (δH_w) using Eq. 2 has been estimated from Holman[14] as

$$\delta H_w = \left(\frac{\partial H_w}{\partial \beta_w}\delta\beta_w\right) \tag{4}$$

where $\delta\beta_w$, denote the errors in the estimation of inlet water fraction. It can be estimated from the errors in measurement of oil and water volumetric flow rate mentioned in Table 1. For this case, the maximum uncertainty in the estimation of H_w for lube oil–water and kerosene-water is 0.022% and 0.11%, respectively.

Experimental observation of flow patterns

The flow patterns as observed from visual inspection and photographic recording are presented in Figures 2 and 3 for lube oil-water and for kerosene-water, respectively. The range of existence of the different flow patterns has been depicted in the form of flow pattern maps in Figures 4 and 5, respectively. The maps are presented with the superficial velocity of oil (U_{so}), and water (U_{sw}) as their abscissa and ordinate. The legends denote the different patterns in the map.

The figures reveal that core-annular flow occupies a central portion in both the flow pattern maps and extends over a

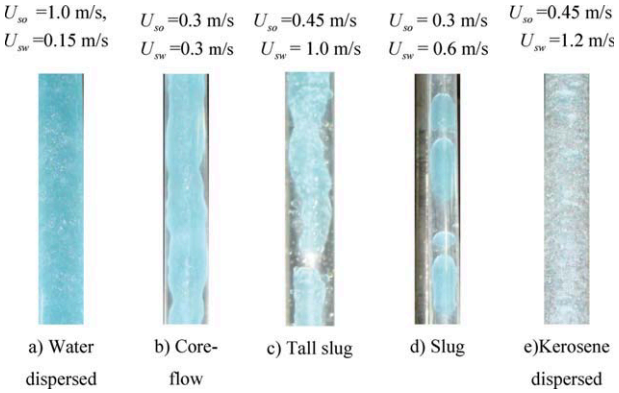

Figure 3. Representative photographs of kerosene-water flow.

[Color figure can be viewed in the online issue, which is available at wileyonlinelibrary.com.]

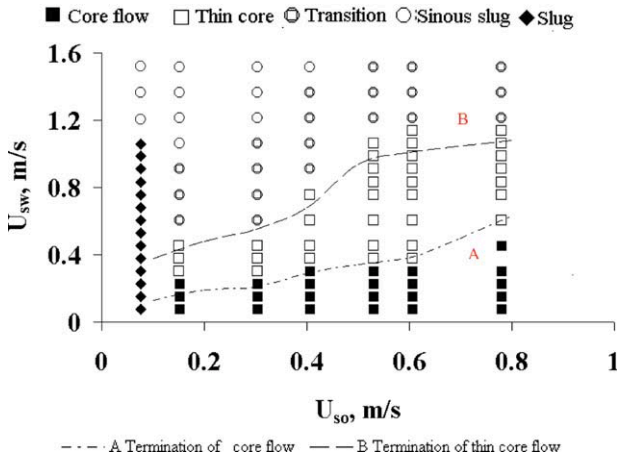

Figure 4. Lube oil–water flow pattern map with transition boundaries.

[Color figure can be viewed in the online issue, which is available at wileyonlinelibrary.com.]

wide range of oil velocities. This is in agreement with the observations by Barnea et al.[15] for gas-liquid systems where they have mentioned that the annular flow pattern is the natural flow regime for two-phase downflow. Furthermore, as mentioned by Joseph et al.[16] there is a strong tendency of high-viscosity oil and water to adjust themselves in such a way so that water moves toward wall. This results in a stable flow configuration from energy consideration. Besides, all the experiments in this study have been performed in a glass pipe of 0.012 m dia. The hydrophilic nature of the wall has also probably assisted in the adherence of a continuous water film on the pipe wall. For both the oils, this flow pattern is characterized by complete separation of the two liquids with oil flowing as a central core and water as a thin continuous film in the annular region between the oil core and the pipe wall. The core is either smooth or wavy and the waviness increases with slip between the phases. In addition, core-annular flow starts above a critical oil velocity for both the oils and this critical velocity is higher for kerosene ($U_{so} \geq 0.3$ m/s) as compared to lube oil ($U_{so} \geq 0.15$ m/s).

For lower oil and/or higher water velocities, the flow pattern is slug flow. It is characterized by alternate passage of oil and water plugs through the test section. At low-oil velocities ($U_{so} < 0.15$ m/s for lube oil–water flow, and $U_{so} \leq 0.3$ m/s for kerosene-water flow), the oil plugs are regular in shape with a clear round nose and tail unlike the jagged wake region observed for gas-liquid cases. Occasionally small oil droplets are found in the water slug entrapped between two successive oil plugs.

However, at high-water flow ($U_{sw} \geq 1.0$ m/s), the oil plugs have a different shape when comparing the flows with lube oil and with kerosene. Such variety in slug flow characteristics has not been reported elsewhere for gas-liquid flow or liquid-liquid flow to the best of the authors' knowledge. Details of the types are discussed later.

The Interfacial Distribution for Lube Oil–Water Flow. It is clear from Figure 4 that the core flow of lube oil becomes thinner and wavier with an increase in water velocity. To understand the influence of interfacial distribution and waviness on the hydrodynamics of flow, attempts have been

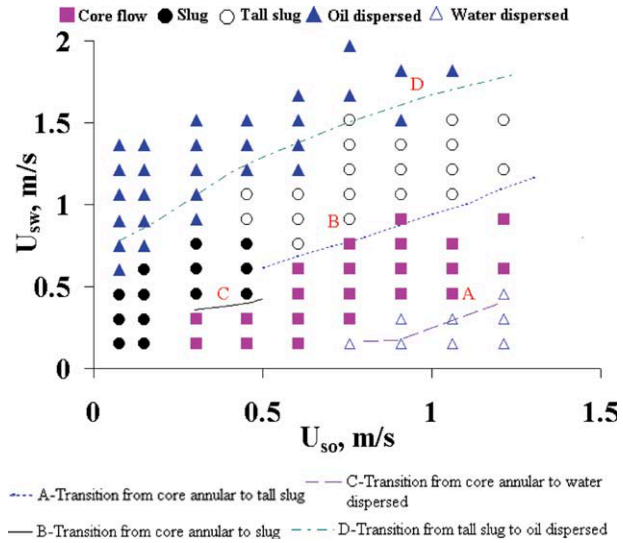

Figure 5. Kerosene-water flow pattern map with transition boundaries.

[Color figure can be viewed in the online issue, which is available at wileyonlinelibrary.com.]

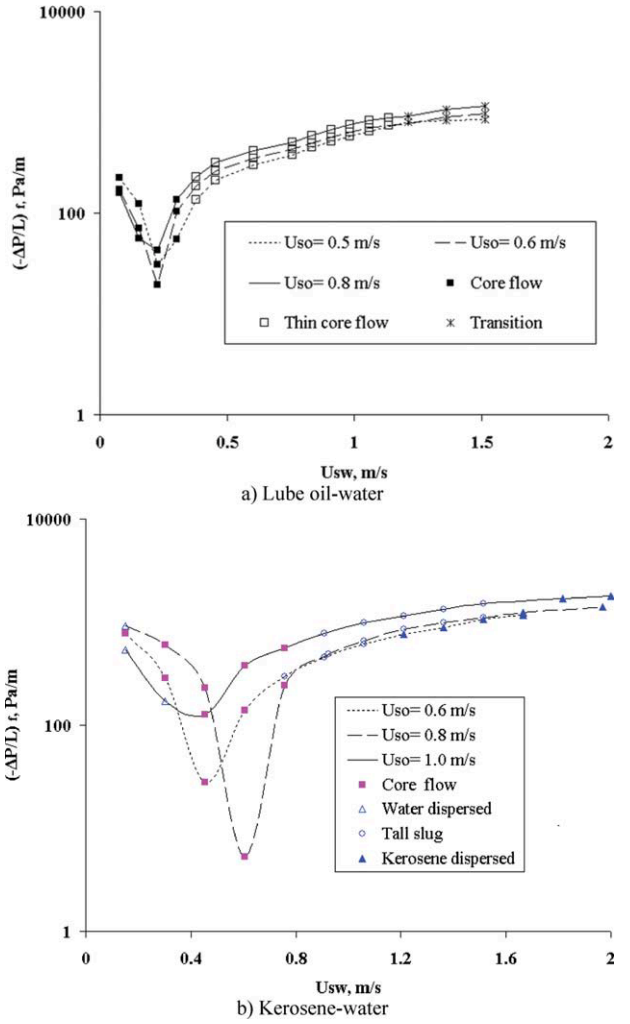

Figure 6. Variation of frictional pressure gradient as a function of water superficial velocity with oil superficial velocity as parameter.

[Color figure can be viewed in the online issue, which is available at wileyonlinelibrary.com.]

made to note the variation of the frictional pressure gradient with water velocity where oil velocity is a parameter. The pressure gradient curves as a function of phase velocities are presented in Figure 6a and b. The data for the different flow patterns have been designated by different symbols to understand the influence of the flow pattern on pressure gradient. The figures show that the pressure gradient decreases in the core annular pattern till it reaches a minimum. Subsequently, it increases continuously with increasing water velocity for other flow patterns. Since one of the primary reasons for establishing core-annular flow is to reduce the power required to pump oil and this advantage ceases to exist with thinning of the oil core, the latter distribution has been distinguished as a separate flow pattern and designated as thin core flow to distinguish it from the conventional core-annular flow pattern. It is characterized by a thinner and wavier core and comparable *in situ* proportions of the two liquids.

As the water velocity is increased further, the waviness increases and the core becomes more and more tortuous until it gets ruptured at certain points by the water phase. The flow passage is marked by the periodic appearance of slug flow with sinuous oil slugs being intercepted by short water bridges. This pattern occurs at a relatively low oil ($U_{so} \leq$ 0.4 m/s), and high-water velocity ($U_{sw} \geq 1.0$ m/s), and has been termed as sinuous slug flow to differentiate it from conventional slug flow.

It may be noted that the transition from thin core flow to sinuous slug flow occurs over a wide range of flow velocities. Under these conditions, the flow appears to be periodic, but the water bridge cannot disrupt the continuity of the oil core completely. Successive oil spirals are accompanied by a thin thread of oil which traverses the short water slugs.

The Interfacial Distribution for Kerosene-Water Flow. The interfacial waves for the kerosene core flow are axisymmetric. When the water velocity is increased, these waves increase in amplitude until they snap the core at different axial locations. However, the water velocity is not high enough to form a stable water slug between successive kerosene slugs. As a result, tall kerosene slugs surrounded by a thin water film appear to remain stacked one above the other as they propagate downward. This flow pattern has been termed tall slug flow in this work.

The tall slugs break down to form oil dispersed flow at higher-water velocities ($U_{sw} > 0.9$ m/s). The distribution of the droplets is relatively uniform in the continuous water phase. The test section appears whitish with fine blue droplets dispersed in it. The droplets become finer as the turbulence of the water phase increases. The reverse, i.e., water dispersed flow occurs at high-oil velocity ($U_{so} <$0.8 m/s), and low-water velocity ($U_{sw} <$ 0.2 m/s). In this case, kerosene forms the continuous phase and water is dispersed in it. The test section appears bluish as can be observed clearly from the photographs (Figure 3). These dispersed flow patterns have not been observed for the high-viscosity oil within this range of experimental conditions.

The physical mechanism governing the termination of core flow

From the aforementioned discussion, it is clear that for the two types of oil used, core flow gives way to completely different interfacial distributions for similar changes of flow velocities. For lube oil–water flow, the core becomes thinner and wavier but does not get disrupted for sufficient increase in water velocity ($U_{sw} <$ 0.6 m/s), whereas the kerosene core gets disrupted by water under these flow conditions. Moreover, it gives way to sinuous slug for lube oil and tall slug flow for kerosene.

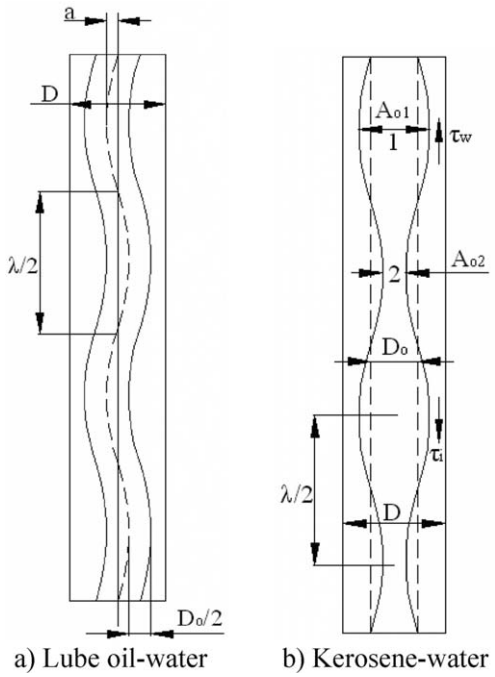

Figure 7. Comparison of core flow.

An increase in interfacial waviness seems to cause the termination of the core flow structure for both the oil viscosity cases. The interfacial waves are asymmetric with respect to pipe axis for the high-viscosity oil case. They resemble the corkscrew waves as reported by Bai et al.[11] for oil–water downflow. On the other hand, the interfacial waves are grossly axisymmetric for the low-viscosity oil case. This explains the difference in the flow patterns observed with increase in water velocity for the two oils used in this study.

To better analyze the difference, enlarged photographs of the core flow for the two oil types along with the schematics have been presented in Figure 7. In the pictorial representation, D and D_o denote the tube diameter and the nominal diameter of the oil core, respectively. λ and α are the wavelength and amplitude of the wavy core. A_{o1} and A_{o2} are the maximum and minimum core area for the axisymmetric wavy core (kerosene-water). The schematic representation explaining the sequence of changes which bring about the termination of the core flow for lube oil–water and for kerosene-water have been presented in Figures 8 and 9, respectively.

Transition for Lube Oil–Water Flow. From Figure 8a it appears that the corkscrew wave makes the lube oil core asymmetric with respect to the pipe axis. An increase in water velocity increases the amplitude of the waves. This stretches the core making it thinner and the onset of thin-core flow occurs when the interfaces of either side crosses the center line of the tube (Figure 8b). On the basis of this observation as noted from repeated photographic visual and photographic studies, it has been postulated that, for thin-core flow, the core radius ($\frac{D_o}{2}$) is smaller in comparison to the amplitude of the wave (a) at the interface. Mathematically, this transition criterion can be described as

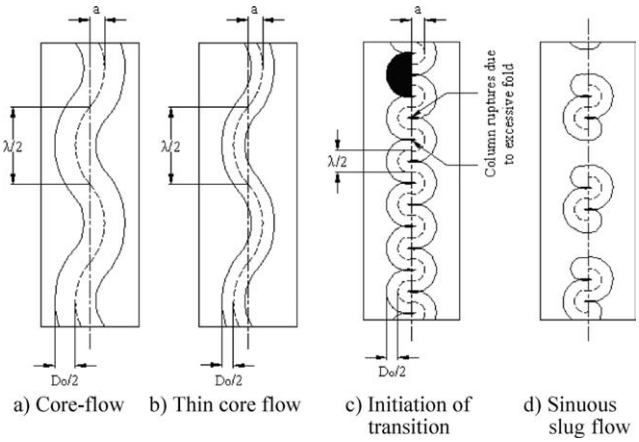

Figure 8. Sequence of transition in lube oil–water flow.

$$a > \frac{D_o}{2} \tag{5}$$

With the increase in water velocity, while the thin core is stretched the core sinuosity increases and the wavelength decreases. It tends to generate folds on both sides of the tube axis (Figure 8c). As the folds come closer, core rupture occurs causing the inception of sinuous slug flow (Figure 8d). This type of situation can be postulated to occur when half of the wavelength becomes smaller than the core diameter. Mathematically this can be expressed as follows for transition from core flow to sinuous slug flow

$$\frac{\lambda}{2} < D_o \tag{6}$$

Transition for Kerosene-Water Flow. For kerosene-water flow, the development of the interfacial waves gives the core an axisymmetric appearance with successive bulging and contractions (Figure 9a). This wavy structure is similar to the bamboo waves that are also observed in core-annular upflow through vertical pipes (Bai et al.[11]). With the increase in water velocity the increased amplitude of the waves causes periodic snapping of the oil core (Figure 9b) when the interface crosses the centerline. In this case the transition criterion is given by the following expression

$$a > \frac{D_o}{2} \tag{7}$$

This suggests that the same criterion marks the termination of core-annular flow for both high-viscosity and low-viscosity oil. However, for the kerosene-water case, it does not disrupt the axisymmetric appearance of the flow passage which is retained also during the tall slug flow (Figure 9c).

On the other hand, when the oil velocity is increased at low-water velocity, the turbulence level becomes sufficiently high to disrupt the water film and to entrain the water into the continuous oil in the form of dispersed droplets. This marks the transition from core-annular flow to water-in-oil dispersed flow. The reverse situation occurs during the transition from tall slug flow to oil-in-water dispersed flow.

Since these transitions are governed by the turbulence level in the continuous phase, they are expected to be independent of the pipe diameter and orientation. Therefore, the model proposed by Hinze[6] and modified by Brauner[7] for dense dispersions is expected to predict the onset of both types of dispersed flow.

Mathematical formulation of the transition criteria

According to the physical mechanisms discussed previously for the development of the transition criteria, it is important to evaluate the amplitude and wavelength of the interfacial waves with respect to the variation in the phase velocities and the change in physical properties. As the first step, one needs to analyze the concentric core flow with a smooth interface to determine the nominal core diameter and superficial velocities. Using Eqs. 5 to 7, mathematical expressions for the transition criteria in terms of known input variables can be obtained. Subsequently, suitable equations are developed for the transition to slug and dispersed flow.

Analysis of Smooth Concentric Core-Annular Flow. A schematic representation of downward core-annular flow with a smooth interface along with the oil and water control volumes is shown in Figure 10. For the ease of analysis, a steady two-dimensional (2-D) model is developed. It is assumed that the velocity fluctuation in radial direction is negligible. Taking the downward direction as positive, the combined momentum equations of both the phases can be obtained as

$$-\frac{\tau_w s_w}{A_w} \pm \tau_i \frac{s_i}{A_w} + \rho_w g = m\tau_i \frac{s_i}{A_o} + \rho_o g \tag{8}$$

The subscripts w and o refer to water and oil, respectively, and i denote the interfacial condition. The terms τ, A, S, and ρ represent shear stress, cross-sectional area, interfacial area and liquid density, respectively. Considering the flow to be fully developed under steady-state condition, A_w and A_o can be expressed in terms of the *in situ* volume fraction of water and the pipe cross-section A as

$$A_w = H_w A \tag{9}$$

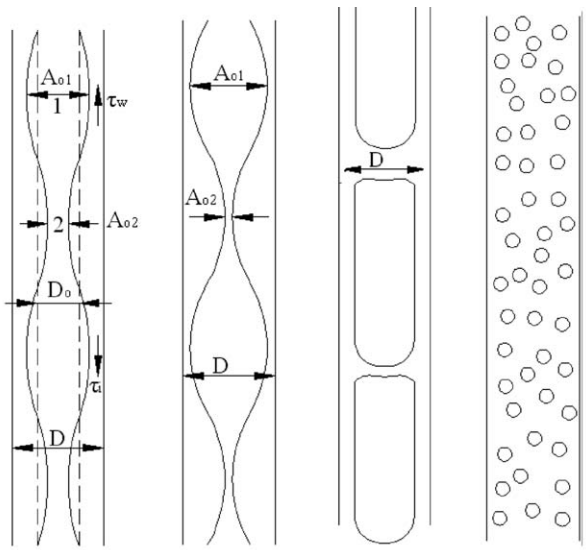

Figure 9. Sequence of transition in kerosene-water flow.

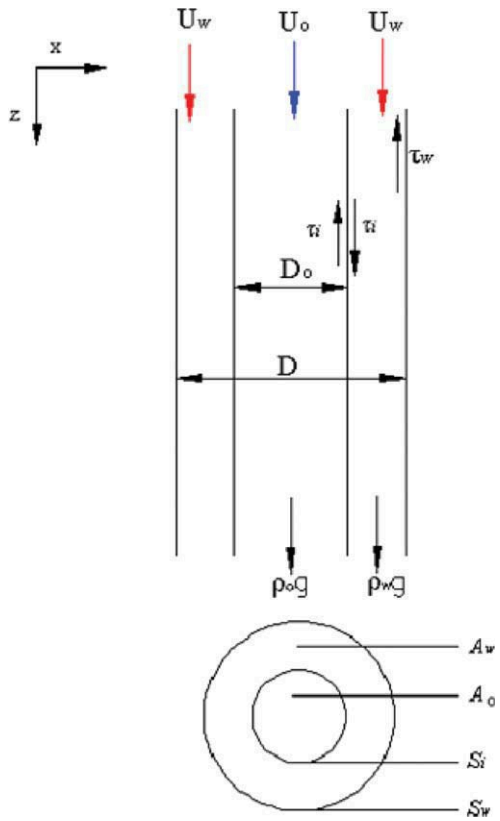

Figure 10. Representation of perfect core-annular flow.

[Color figure can be viewed in the online issue, which is available at wileyonlinelibrary.com.]

$$A_o = (1 - H_w)A \tag{10}$$

For a circular pipe

$$S_w = \pi D \quad \text{and} \quad S_i = \pi D_o \tag{11}$$

where D is the pipe diameter, and D_o is the diameter of oil core.

For a smooth interface D_o is

$$D_o = D\sqrt{1 - H_w} \tag{12}$$

Substituting Eqs. 9–12 into Eq. 8 we get

$$(\rho_o - \rho_w)g + \frac{4}{D}\frac{\tau_w}{H_w}\mathrm{m}\tau_i\frac{4}{D}\sqrt{1 - H_w}\left(\frac{1}{1 - H_w} + \frac{1}{H_w}\right) = 0 \tag{13}$$

Since the wall is always wetted by water only, the wall shear can be expressed as

$$\tau_w = \frac{1}{2}f_w\rho_w U_w^2 \tag{14}$$

where

$$f_w = m(\mathrm{Re}_w)^{-n} \tag{15}$$

and

$$\tau_w = \frac{1}{2}f_i\rho_i(U_o - U_w)^2 \tag{16}$$

$$f_i = m(\mathrm{Re}_i)^{-n} \tag{17}$$

ρ_i, U_i, μ_i can be equated to ρ_o, U_o, μ_o for $U_o > U_w$, and ρ_w, U_w, μ_i for $U_w > U_o$. μ_o is the viscosity of oil phase, and U_o, U_w are the *in situ* velocities of oil and water phase, respectively. The constants n and m are $m = 16$, $n = -1$ for laminar flow, and $m = 0.079$, and $n = -0.25$ for turbulent flows.

Substituting Eqs. 14–17 into Eq. 13, the following equation is obtained

$$(\rho_o - \rho_w)g + \frac{2}{D}(\mathrm{Re}_w)^{-n}\rho_w\frac{U_w^2}{H_w} \mp \frac{2}{D}\sqrt{1 - H_w}m(\mathrm{Re}_i)^{-n} \times \left(\frac{1}{1 - H_w} + \frac{1}{H_w}\right)\rho_i(U_o - U_w)^2 = 0 \tag{18}$$

This equation can be solved iteratively to obtain the *in situ* water fraction H_w for a given pair of phase velocities. Substitution of the value of H_w into Eq. 12 gives D_o.

Imposition of Waviness in the Core From the previous discussion it is clear that the waviness in the interface of the oil core plays the most crucial role in its transition. For two parallel streams with a difference in velocity, the Kelvin-Helmholtz instability is the root cause of the wavy interfacial structure. Nevertheless, the manifestation of such waviness is different in kerosene-water flow as compared to lube oil–water flow. A rigorous analysis of the wave instability requires computational fluid dynamic simulations. For example, the axisymmetric, bamboo wave instability for core-annular flow has been analyzed by Bai et al.[17], Ooms and Poesio[18] and Ooms et al.[19] and the corkscrew wave instability was analyzed by Bai et al.,[11] Hu and Patankar[20] and Huang and Joseph.[21] In the aforementioned studies detailed computational simulations were carried out. In this work, we propose a simplified analysis so that a closed form expression for the transition criteria could be obtained.

For ease of analysis, it is assumed that the actual interfacial wave velocity is proportional to the one corresponding to a plane interface. The plane sinusoidal wave has a velocity C_v, wavelength λ, and amplitude a. The equation of the sinusoidal waves at the oil–water interface can be expressed as

$$x = a\sin\left(\frac{2\pi z}{\lambda}\right) \tag{19}$$

where, x and z are the transverse and axial distances, respectively. Using the analysis of Lienhard and Lienhard[22] for the Kelvin Helmholtz instability, the wavelength λ for this case of two-fluid flow can be expressed in terms of the slip between the phases

$$\lambda = \frac{2\pi\sigma}{\rho_o(U_o - U_w)^2} \tag{20}$$

The transition equations for lube oil–water flow

The core dia. D_o, and wave characteristics λ and a when substituted in Eqs. 5 and 6 provides the equations for the transitions to thin-core flow and to sinuous-slug flow.

The Transition to Thin-Core Flow.

For the transition criterion to thin-core flow in Eq. 5, D_o can be obtained from Eq. 12 when substituting H_w from Eq. 13, and a is obtained by differentiating Eq. 19 viz

$$\frac{dx}{dt} = \frac{a2\pi}{\lambda}\cos\left(\frac{2\pi z}{\lambda}\right)\frac{dz}{dt} \tag{21}$$

This equation gives C_v as the velocity of the wave in the axial direction (z) for unit velocity in radial direction. Thus, for $\frac{dx}{dt} = 1$

$$\frac{dz}{dt} = C_v \tag{22}$$

Substituting Eq. 22 into Eq. 21, we get

$$C_v = 1 \Big/ \left(\frac{a2\pi}{\lambda}\cos\left(\frac{2\pi z}{\lambda}\right)\right) \tag{23}$$

The average phase velocity during half the cycle ($\lambda = 0$ to $\lambda/2$) [$(C_v)_{avg}$] can then be obtained as

$$(C_v)_{avg} = \frac{\lambda}{4a\pi} \tag{24}$$

Equation 24 estimates (a) for a given operating conditions, where λ can be obtained using Eq. 20. The flow velocities which yield a value of (a) greater than D_o cause the transition to thin-core flow.

The Transition from Thin-Core Flow to Sinuous Slug Flow

To obtain the criterion for the termination of thin-core flow as given by Eq. 6, the values of D_o and λ can be obtained from Eqs. 12 and 20, respectively. For a particular combination of the oil and water velocities, giving a wavelength that is less than the diameter of the smooth core, the thin-core regime breaks down to form sinuous slug flow.

The Transition Equations for Kerosene-Water Flow. The mathematical equations for predicting the transition from core annular flow to tall slug flow, regular slug flow and water dispersed flow have been obtained as follows.

The transition from core annular flow to tall slug flow

To estimate the wave amplitude of the interfacial waves an axisymmetric wave has been considered. The difference in pressure between points 1 and 2 in Figure 7b is obtained by applying Bernoulli's equation separately in the oil and the water phase.

Following the methodology of Al-Wahaibi and Angeli[9] the critical amplitude at which the interfacial waves become unstable has been obtained by balancing the pressure across interface at points 1 and 2 by surface forces corresponding to maximum axial curvature. This results in the following equation

$$\begin{aligned}&\frac{1}{2}\rho_w\left[(U_w - C_v)^2\left(\left(\frac{A_w}{A_{w2}}\right)^2 - \left(\frac{A_w}{A_{w1}}\right)^2\right)\right]\\ &+\frac{1}{2}\rho_o\left[(U_o - C_v)^2\left(\left(\frac{A_o}{A_{o1}}\right)^2 - \left(\frac{A_o}{A_{o2}}\right)^2\right)\right]\\ &\qquad -\frac{\lambda}{2}g(\rho_w - \rho_o) - \frac{8\pi^2 a}{\lambda^2}\sigma - 4\frac{\sigma}{D_o} = 0\end{aligned} \tag{25}$$

The wavelength in the aforementioned equation is calculated using Eq. 20. The wave velocity C_v can be obtained from (Wallis[23])

$$C_v = \left(\frac{\partial U_{sw}}{\partial H_w}\right)_J \tag{26}$$

where

$$U_{sw} = \frac{Q_w}{A} \tag{27}$$

The corresponding areas at plane 1 and 2 are given as

$$A_{o1} = \frac{\pi}{4}(D_o + 2a)^2 \tag{28}$$

$$A_{o2} = \frac{\pi}{4}(D_o - 2a)^2 \tag{29}$$

$$A_{w1} = A - A_{o1} \tag{30}$$

$$A_{w2} = A - A_{o2} \tag{31}$$

Substituting Eqs. 26–31 into Eq. 25 we can obtain a by an iterative solution.

If Eq. 25 gives "a" such that $2a > D_o$, the core is unstable and tends to break and form tall slugs.

An additional attempt has been made to check whether A_{o1}, as given by Eq. 28 is less than the pipe cross-sectional A. This has been done to ensure that the kerosene core does not wet the pipe wall and the transition to tall slug occurs.

Termination of Core Annular Flow to Slug Flow at Low-Water Velocity For kerosene-water flow the transition from core-annular flow to slug flow takes place with increasing water velocity for a limited range of oil velocities (0.3 m/s $\leq U_{so} \leq$ 0.45 m/s). Barnea et al.[15] have suggested that for air–water downflow the transition from annular flow to slug flow occurs at $H_w = 0.35$. In this study H_w has been obtained from an iterative solution of Eq. 13 for a pair of kerosene and water superficial velocities. A good match with experimental data is obtained for $H_w = 0.3$. Therefore, it is postulated that the critical water holdup fraction marking the transition from core-annular flow to slug flow for kerosene-water cases is $H_w = 0.3$.

Transition from Core-Annular Flow to Water Dispersed. The transition from core-annular flow to water dispersed flow at high-oil and low-water velocities can be predicted if the condition at which dispersion persists is analyzed. Taking the queue from Brauner[6] it is suggested that dispersion can exist if $(d_{\max}) \leq d_{crit}$.

According to K-model of Hughmark,[24] the critical diameter (d_{crit}) for a two-fluid system with an Eötvös number ($Eo = \frac{(\rho_w - \rho_o)gD^2}{8\sigma}$) lower than 5 can be obtained from the analysis provided by Brodkey.[25] Accordingly in this case

$$d_{crit} = \left[\frac{0.4\sigma}{(\rho_w - \rho_o)g}\right]^{1/2} \tag{32}$$

where σ is the interfacial tension.

Consequently, the transition curve is obtained as $d_{\max} = d_{crit}$ where the continuous phase is kerosene and the dispersed phase is water. The maximum diameter ($d_{\max}$) can be obtained from the equation proposed by Brauner[6] as

$$\left(\frac{d_{\max}}{D}\right) = 7.61C(we)_o^{-0.6}(\mathrm{Re})_o^{0.08}\left(\frac{\beta_w}{1-\beta_w}\right)^{0.6}\left[1 + \frac{\rho_w}{\rho_o}\frac{\beta_w}{1-\beta_w}\right]^{-0.4} \tag{33}$$

In Eq. 33, C is a constant, β is the inlet volume fraction of the dispersed phase, We, Re are the respective Weber and

Reynolds numbers of the continuous phase. For this case with oil as the continuous phase

$$\mathrm{Re}_o = \frac{DU_{so}\rho_o}{\mu_o} \tag{34}$$

and

$$We_o = \frac{\rho_o U^2{}_{so} D}{\sigma} \tag{35}$$

The Transition from Tall Slug Flow to Oil Dispersed Flow. This transition can be described by a similar aforementioned analysis, but now by considering water as the continuous phase and kerosene as the dispersed phase. The transition criterion is obtained as $(d_{\max}) < d_{crit}$; where

$$\left(\frac{d_{\max}}{D}\right) = 7.61C(We)_w^{-0.6}(\mathrm{Re})_w^{0.08}\left(\frac{\beta_o}{1-\beta_o}\right)^{0.6}\left[1+\frac{\rho_o}{\rho_w}\frac{\beta_o}{1-\beta_o}\right]^{-0.4} \tag{36}$$

Validation of the transition analysis

The predictions for the transition criteria as derived above are compared with the experimental flow pattern maps for lube oil–water and kerosene-water flow in Figures 4 and 5. In Figure 4 (for lube oil) curve A denotes the prediction for the transition to thin core flow and curve B is the prediction for the transition from thin core-annular flow to sinuous slug flow. There is a good agreement between the predicted and the experimental transition curves.

The inception of core-annular flow from water dispersed flow for the kerosene-water case in Figure 5 is predicted from equation $d_{\max} = d_{crit}$ and denoted by curve A. Similarly, Curve B denotes the transition of core-annular flow to tall slug flow. In the same figure, curve C represents equation $H_w = 0.3$, which governs the transition from core-annular flow to slug flow. Curve D denotes the transition from tall slug to oil dispersed flow.

The close agreement between experiment and theory for all the cases supports the validity of the proposed mechanisms.

Conclusion

We have carried out laboratory experiments with flow visualization for various flow patterns for oil–water downflow through a vertical pipe. To investigate the effect of oil viscosity on the down-ward transport of the oil–water mixture two different oils, namely lube oil and kerosene, with a large difference in viscosity, have been chosen. The experimental observations reveal that the flow regime is predominantly core-annular flow for both the high-viscosity and the low-viscosity oils, which gives a transition to slug flow when the water flow rate is increased and/or the oil flow rate is decreased.

The appearance of slug flow in oil–water transport at low-phase velocities is similar to slug flow observed for gas-liquid systems. However, slug flow appears to be distinctly different at high-oil flow rates. For lube oil–water flow, sinuous slugs are observed while tall slugs are found for kerosene-water flow. Such typical slug structures have not been reported so far for gas-liquid or for liquid-liquid cases to the best of the authors' knowledge.

Interfacial waves have been observed for both lube oil–water and kerosene-water downflow when the water velocity is increased. It is postulated that the transition from core-annular flow to slug flow occurs due to an increase in the interfacial waviness in both the cases. The wave structures are grossly different in the two situations. Axisymmetric bamboo waves occur for kerosene-water downflow, and the core structure is asymmetric and resembles a corkscrew wave for lube oil–water downflow. In both the cases snapping of the wavy core gives way to slug flow. However, the high-viscosity lube oil core gets stretched and folded before snapping. As a result, a new flow regime—denoted as "sinuous slug"—flow is observed.

Based on these observations, the same transition criterion, i.e., the wave amplitude must exceed the core radius marks the termination of the core-annular flow for both the cases. However, as the structure of the wavy cores are different, separate analyses are required to derive the transition criterion. Simple mathematical models have been derived to quantify the transition boundaries. The derived transition boundaries show a reasonably good agreement with the experimental observations.

It may be noted that this study has reported the effect of phase superficial velocities and oil properties on the flow patterns during oil–water downflow through vertical pipe. Further investigations are necessary to understand the effect of pipe diameter and surface wettability on oil–water downflow.

Literature Cited

1. Brauner N, Moalem Maron D. Stability analysis of stratified liquid-liquid horizontal flow. *Int J Multiphase Flow*. 1992;18:103–121.
2. Russell TWF, Hodgson GW, Govier GW. Horizontal pipeline flow of oil and water. *Can J Chem Eng*. 1959;37:9–17.
3. Guevara E, Zagustin K, Zubillaga Y, Trallers JL. Core-annular flow: the most economical method for the transportation of viscous hydrocarbons. 4th Int. Conference on Tar-Sands and Bitumens; 1988; Edmonton, Alberta, Canada; paper No. 194.
4. Grassi B, Strazza D, Poesio P. Experimental validation of theoretical models in two phase high viscosity ratio liquid-liquid flows in horizontal and slightly inclined pipes. *Int J Multiphase Flow*. 2008;34: 950–965.
5. Trallero JL. Oil–Water Flow Patterns in Horizontal Pipes [Ph.D. Thesis]. University of Tulsa; 1995.
6. Brauner N. The prediction of dispersed flows boundaries in liquid-liquid and gas-liquid systems. *Int J Multiphase Flow*. 2001;27:885–910.
7. Hinze J. Fundamentals of the hydrodynamic mechanism of splitting in dispersion processes. *AIChE J*. 1955;1:289–295.
8. Brauner N. *Liquid-liquid two-phase flow systems*. In: Bertola V, editor. *Modeling and Control of Two-phase Flow Phenomena*. CISM Center: Udine, Italy; 2002.
9. Al-Wahaibi T, Angeli P. Transition between stratified and non-stratified horizontal oil–water flows: part I (stability analysis). *Chem Eng Sci*. 2007;62:2915–2928.
10. Sotgia G, Tartarini P, Stalio E. Experimental analysis of flow regimes and pressure drop reduction in oil–water mixtures. *Int J Multiphase Flow*. 2008;34:1161–1174.
11. Bai R, Chen K, Joseph DD. Lubricated pipelining: stability of core-annular flow: Part 5. Experiments and comparison with theory. *J Fluid Mech*. 1992;240:97–132.
12. Liu L, Matar OK, Hewitt GF. Laser-induced fluorescence (LIF) studies of liquid-liquid flows. Part II: Flow pattern transitions at low liquid velocities in downwards flow. *Chem Eng Sci*. 2006;61:4022–4026.
13. Arney MS, Bai R, Guevara E, Joseph DD, Liu K. Friction factor and hold up studies for lubricated pipelining - I. experiments and correlations. *Int J Multiphase Flow*. 1993;19:1061–67.
14. Holman JP. *Experimental Methods for Engineers*. New York: McGraw-Hil; 1989.
15. Barnea D, Shoham O, Taitel Y. Flow pattern transition for vertical downward two phase flow. *Chem Eng Sci*. 1982;37:741–744.
16. Joseph DD, Bai R, Chen KP, Renardy YY. Core-annular flows. *Annu Rev Fluid Mech*. 1997;29:1–30.

17. Bai R, Kelkar K, Joseph DD. Direct simulation of interfacial waves in a high viscosity ratio and axisymmetric core annular flow. *J Fluid Mech*. 1996;327:1–34.
18. Ooms G, Poesio P. Stationary core-annular flow through a horizontal pipe. *Phys Rev E*. 2003;68:066301.1–7.
19. Ooms G, Vuik C, Poesio P. Core-annular flow through a horizontal pipe: hydrodynamic counterbalancing of buoyancy force on core. *Phys Fluids*. 2007;19:092103.1–092103.17.
20. Hu HH, Patankar N. Non-axisymmteric instability of core-annular flow. *J Fluid Mech*. 1995;290:213–234.
21. Huang A, Joseph DD. Stability of eccentric core-annular flow. *J Fluid Mech*. 1995;282:233–245.
22. Lienherd IV JH, Lienherd V JH. *A Heat Transfer Textbook*. Cambridge, MA: Phlogiston Press; 2005.
23. Wallis GB. *One Dimensional Two Phase Flow*. New York: McGraw Hill Book Co., Inc; 1969.
24. Hughmark GA. Drop breakup in turbulent pipe flow. *AIChE J*. 1971;17:1000.
25. Brodkey RS. *The Phenomena of Fluid Motions*. Reading, MA: Addison-Wesley; 1969.

Manuscript received Aug. 31, 2010, and revision received July 5, 2011.